



Coherent Population Trapping with Quantum Interference: Mechanisms and Applications

Dr.Niranjana A R

Assistant Professor of Physics, GFGC Koppa-577126, Chikkamagaluru District,
Karnataka State, INDIA.

Abstract

In quantum physical research, quantum blockage is commonly understood as a typical outcome of wave-molecule duality at the atomic level. Because of the interaction with directly directed laser light in this design, I have investigated the Cognizant Populace Catching (CPT) impact that occurs in the ^{87}Rb D1 line. A key component of this cooperation plot is the quantum impedance between dull states, since the design of the energized state influences rationality profoundly. Here, the implications of the laser optical detuning for the CPT reverberation are investigated. The commitment of a few dim states to the general sign can be calculated by using hypothetical and exploratory data. Considering these findings, I have focused on the sign's correlation with the laser line width and pressure extension of the optical progress, and one may determine the circumstances in which neither of the variables reduces the CPT reverberation.

Keywords: Quantum Interference, Coherent Population Trapping

DOI Number: 10.48047/nq.2022.20.6.NQ23040

NeuroQuantology2022;20(6): 101596-101605

1. INTRODUCTION

Theoretical and practical investigations of the Coherent Population Trapping (CPT) phenomena were carried out during the 1970s. These groundbreaking investigations suggest that a quasi-resonant, two-frequency, coherent light field interacts with the ground states to produce the CPT effect. Both the nuclear framework state and the light bar's propagation through the medium are impacted by CPT and associated anomalies (such as electromagnetically induced ingestion and straightforwardness).

In this way, the quantum system is configured in a condition that does not absorb light, called the dark state. For example, the energy levels of alkali atoms are grouped in a way. In order to capture CPT resonances, the study modifies the recurrence contrast between two sections of the extraterrestrial electromagnetic field surrounding the ground state recurrence parting value. The components of the CPT resonances have

several uses, such as atomic magnetometry, atomic repeat standards, beat delaying, and tension for optical memory.

The test in the usage of this effect in those applications is the inadequacy of the CPT impact, which often only aims for an inconspicuous vacillation in the light of the nuclear example. Recently, a number of creative light-iota collaboration strategies have been tried to circumvent this requirement. Specifically, the authors' work shows that the CPT effect can be amplified greatly by the so-called CPT configuration. Here, two co-propagating linearly polarized laser beams resonate with the Rb isotope transitions to $5\ 2P_{1/2}$ $F = 1$. Instead of the prominent CPT reverberation produced by a circularly stimulated laser field, the faint state results from a vectorial coupling ($\Delta m_F = 0$) due to a directly stimulated and circularly stimulated laser field, respectively.

As the ground and activated nuclear levels are constructed, a theoretical analysis of a four-

101596



level structure that tackles the CPT reverberation has been presented. These frameworks are appealing because of their genuine ability to alter optical qualities via quantum obstruction between two dull states, such as by using the neighbourhood dim state stage or the periods of laser radiations. In the ongoing work, I have looked into the method for acting on the CPT resonance that takes place inside the hyperfine change complex of the Rb D1 line. The architecture of the energetic hyperfine states, which is explored in further detail in Segment II near the information understanding model, does not completely determine the CPT reverberation. Complete analysis is done on the laser linewidth, homogeneity expansion, pressure widening (caused by the cushion gas in the cell), and CPT resonances. It should be evident that surveying has not received as much attention as it has thus far.

2. LITERATURE REVIEW

Vartanyan et al. (2017) provide a detailed investigation of coherent population trapping in quantum interference events. They describe the fundamentals of CPT and emphasize its significance for clock construction, precision spectroscopy, and quantum memory systems. This research looks at a number of theoretical and experimental components to provide light on the physics behind CPT and its potential for practical applications. If one wishes to understand the foundations of CPT and how it connects to quantum mechanics, their work is a fantastic place to start.

The optical Bloch equations for incoherent light scattering were proven by groundbreaking experiments carried out by Lett et al. in 1988. The theoretical basis for comprehending CPT and associated quantum

3. RESEARCH METHODOLOGY

This review utilizes two particular light sources: a pair of phase-locked extended cavity diodes (PLECD)

interference phenomena was established in large part by this study. They gave empirical support to the theoretical predictions by empirically proving the optical Bloch equations, and they opened up new research directions for investigating coherent processes in atomic systems.

Rubidium vapours were studied by Akulshin and Sidorov (2008) for CPT and electromagnetically induced transparency (EIT). This study examines the relationship between CPT and EIT and illustrates how quantum interference affects atomic absorption characteristics. Their research advances knowledge of CPT in multi-level atomic systems and its potential uses in quantum optics and information processing.

Hakhumyan et al. (2013) concentrated on CPT and EIT in atomic systems with three levels of ladders. Their research broadens the study of quantum interference to encompass more intricate atomic structures and sheds light on the function of dark states and quantum coherence in these kinds of systems. By taking into account different atomic configurations and their significance in quantum memory and atomic clock technologies, this research broadens the range of CPT applications.

In three-level systems, Zhu, Lin, and Muga (2014) investigated coherent population trapping via adiabatic fast passage. This study presents a novel method for regulating CPT via adiabatic methods, potentially opening up new possibilities for quantum state control. By offering different techniques for producing and making use of coherent population trapping, their study makes a contribution to the developing fields of CPT and quantum interference.

101597

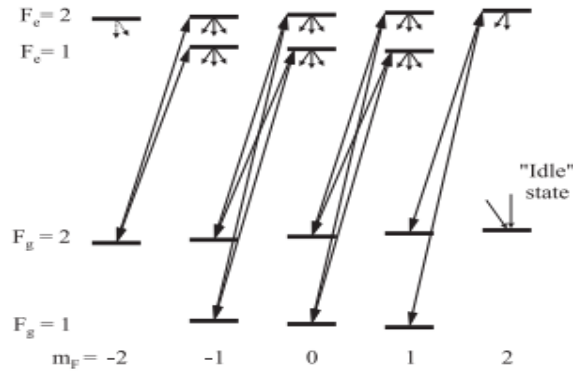


Figure1:Diagrammatic representation of the light-induced transitions that stimulate the hf transitions associated with the D1 line of the Rb isotope and lead to the +- + CPT resonance.

Current-modulated lasers, such as vertical cavity surface emitting lasers, or ECDLs. The PL-ECDLs show pure dichromatic fields with a small line width, roughly speaking. On the other hand, the balanced VCSEL has a wider line width and a multi-recurrence range. Section IV provides a detailed explanation of the experimental setup and laser sources.

3.1. Compact atomic clocks using the CPT resonance

Diminished CPT-based atomic timepieces have been visible for a few years now, spaced sufficiently apart. The most well-known method for CPT excitation is the cooperation of Cs or Rb isotopes with a circularly structured laser field, in which the two recurrence components of the driving laser field (henceforth referred to as σ - σ CPT) cause either + or changes. A typical excitation process for the ⁸⁷Rb D1 complex with hyperfine alterations (the ambiguous situation I will discuss for the configuration) is shown in Figure 1. A delicate attractive field of a many T that is adjusted toward laser transmission is utilized to lighten the decadence of the Zeeman sublevels for this situation. The issue of this association plot relies upon the way that the state |F_g = 2, m_F = 2 | isn't related with the excitation cycle. The populace is gathered into this inactive state because of the optical siphoning impact achieved by the

$$\rho_{ij} = -\frac{i}{\hbar} \sum_k [H_{ikp} \rho_{kj} - H_{kj} \rho_{ip}] + \sum_{k,l} T_{ij,kl} \rho_{kl} \quad (1)$$

The atomic unperturbed Hamiltonian, \hat{H}_0 , and the interaction operator, \hat{V} , are the two terms that make up the Hamiltonian, H, which has the formula., $\hat{H} = \hat{H}_0 + \hbar\hat{V}$. $\Gamma_{ij,kl}$ The relaxation matrix element i, j, k, and l describes the relaxation processes. The following may be expressed as the two-frequency laser field:

isotropic unconstrained rot of the energized states, which fills in as a misfortune system for the clock reference reverberation.

Then again, not at all like the CPT setup depicted in segment II, which has no inactive states, the state populace is evenly focused at the Zeeman sublevel and has a quantum number of m_F = 0. This can be subjectively perceived on the grounds that there is no net exchange of precise energy from the straightly spellbound light to the particles during the excitation stage. A higher sign to-clamor proportion is consequently expected with higher laser powers and lower cushion gas pressures. Because of this property, the CPT reverberation is areas of strength for a for an elite presentation minimal nuclear clock (an exhaustive report is distributed in).

3.2. Scheme Interaction and Modelling Scheme

Using a model based on the thickness lattice approach—which is explained in full in the reference—was the aim of the data analysis. In this section, I'll outline the basic approach and give a clear example of the results that are important to our conversation. Examine an ⁸⁷Rb isotope stimulated by a double recurrence laser field in phase with the hf-changes of the D1 line. 1 and 2 are equal to 5 2P1/2 F_e and 5 2S1/2 F_g. For this system, the density matrix evolution is given by



$$\vec{E}(z, t) = \sum_{j=1,2} \left[\frac{\vec{E}}{2} \exp[i(\omega_j t + \sigma_j(t) - k_j z)] \right] + C, C \dots \quad (2)$$

It's interesting to note that the stage varieties $\phi_j(t)$ are used to characterise the laser line's width. The following formulae can be used to determine the weak absorption of laser energy by an optically thin gas cell:

$$\Delta P = P_{exc} h\nu_{opt} \gamma N_a, \quad (3)$$

In an optically weak gas cell, where the connection Hamiltonian $h\nu_{ij}$ framework pieces are intended to maintain stability along the optical path, ρ_{exc} isn't a part of the optical path due to a weak retention. The gas cell becomes optically dense at high temperatures. As a result, the dark states and density matrix elements depend on the quantity of light travelling along the optical channel. Due to the intimate relationship between I have employed an optically thick ^{87}Rb vapour cell for this study. The optical path is then separated into a series of progressive segments in the model. The thickness grid is created assuming that each thin layer's electrical fields ($E_i = \text{const.}$) have the same values. The fluctuations of the E-fields within the layer are then determined using the Maxwell equations for the slowly varying E-field amplitude and phase. The thickness lattice of the adjacent layer is then determined using the new E-field that is generated from the preceding layer. The next

parts all follow the same format. In the quantitative computations, we don't account for variations in the cross over force appropriation. However, we can reproduce the results of the experiment using this simple phenomenological method (see Section IV). In the examples that follow, the initials g , and g' , and e stand for the ground and excited state Zeeman sublevels. Keep in mind that when the changes $|g_i| |e_i$ and $|g' | |e_i$ are animated at the same time, a dim state may result since g and g' have distinct hyperfine ground states in their respective locations. The light power spent on the off chance that the laser field power is substantially lower than as far as is practicable for each optical change and the phone is optically thin (c.f. condition 3), corresponds to the absolute energised state population (exc). The excited state density matrix element is connected using the rotating wave approximation without taking into consideration the fast oscillating $\sim O(\omega_i + \omega_j)$ and $\sim O(2\omega_i)$ etc.

101599

$$\rho_{exc} = \sum_{e,g,g'} \left[\frac{V_{eg}^0 V_{ge}}{\gamma} (G_{ge} + G_{ge} + i(F_{ge} - F_{ge})) \right] \rho_{gg} \quad (4)$$

to the components of the ground state density matrix that may be obtained by solving the following system of equations:

$$\begin{aligned} \rho_{gg} = & -i\rho_{gg'}(\omega_{gg'} - \omega_g + \omega_{\omega_{g'}}) + \tau \left(\frac{1}{8} \delta_{gg'} - \rho_{gg} \right) \\ & \sum_{g'',e} \left[\frac{V_{ge} V_{eg''}}{\gamma'} (G_{g'} + iF_{g'e}) \right] \rho_{g''g'} - \\ & \sum_{g'',e} \left[\frac{V_{g''e} V_{eg'}}{\gamma'} (G_{ge'} + iF_{ge}) \right] \rho_{gg''} + \frac{\delta_{gg'}}{8} \\ & \sum_{e,g'',g'''} \left[\frac{V_{g''e} V_{eg''''}}{\gamma'} (G_{g''e} + G_{g''e} + i(F_{g''e} - F_{g''e})) \right] \end{aligned} \quad (5)$$

$$\sum_g \rho_{gg} = 1 \quad (6)$$

Here, γ' is the optical clarity decay rate, ρ_{eg} ; $\delta_{gg'}$ $h\nu_{ij}$ s the lattice of the communication in the edge pivoting with the fitting laser recurrence part, and ω_g is the Kronecker delta. The repeat of the laser part that helps out level g is $\omega_{gg'}$. and the repeat opening between levels $|g_i$ and $|g' |$ is $\omega_{gg'}$. The ground state loosening up rate, tended to by, is dependent upon the cell's temperature, support gas' sort and strain, cell's estimation, laser power, and laser emanates math. The free fit limit in our proliferation, not entirely set in stone from the data, is called. In, the creators exhibit that the optical



soundness rot not set in stone by the laser linewidth L the unconstrained unwinding rate Γ which is for Rubidium $\approx 2\pi \cdot 5.6$ MHz, and the tension expanding $\gamma c_{,,}$, which is impacted by the sort of cushion gas and the cell's cradle gas pressure γ' :

$$\gamma' = \frac{\gamma_{sp} + \gamma_e + \tau\tau_l}{2} \quad (7)$$

We ought to analyse a general single change $|g\rangle \leftrightarrow |e\rangle$. to appreciate the actual meaning of γ' . At the point when this progress is invigorated by a laser light field of linewidth Γ_L , a homogenous extended profile that might be described by a Lorentzian bend of linewidth γ' . ' is created (figure 2).

$$G_{ge} = \int_{-\infty}^{+\infty} \frac{(\gamma')^2 M(v)}{(\gamma')^2 + (\delta_L^{eg} - kv)^2} dv$$

$$F_{ge} = \int_{-\infty}^{+\infty} \frac{\gamma'(\sum_L^{eg} - K_v)M_v}{(\gamma')^2 + (\delta_L^{eg} - kv)^2} dv \quad (8)$$

where $M(v)$ indicates the circulation of nuclear speeds and δ_L^{eg} means the laser detuning. While the coefficient F_{ge} makes it possible to conclude the shift of the resonation repeat, the coefficient G_{ge} is comparing to significant solid areas for how single optical advancement $|g\rangle \leftrightarrow |e\rangle$ is. To achieve our targets, we centrearound the coefficient G_{ge} which is schematically depicted in figure 2. The hazy situation that G_{ge} is relative to is made by consolidating the Doppler profile, which is portrayed by a

Gaussian bend $M(v)$ of linewidth D , and the homogeneous profile, which is portrayed by a Lorentzian bend $L(kv)$ of linewidth γ' . When various $|g\rangle \leftrightarrow |e\rangle$ changes are stirred, G_{ge} portrays how each progress adds to the general excitation process. The earlier examination for a solitary optical change presently incorporates a dim state. The advances from both ground states $|g\rangle$ and $|g'\rangle$ towards a comparable stimulated level $|e\rangle$ ought to be begun by two photons meanwhile to make the dull state.

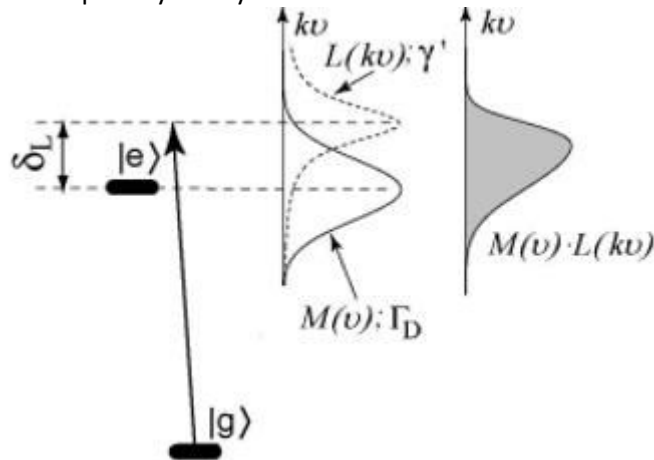


Figure 2: diagrammatic portrayal of a progress ($|g\rangle \leftrightarrow |e\rangle$). as well as a uniform expanding profile (Lorentzian bend $L(kv)$ in ran linewidth γ'). "Leg" is the laser detuning. The progress' Doppler profile, $M(v)$, is portrayed by a strong line of a Gaussian bend with linewidth D . The dim region under the two curves' thing, $L(kv) M(v)$, is comparative with G_{ge} in condition (8).

Coherent components of the electromagnetic field, also known as the electromagnetic field components, exhibit very little relative frequency jitter. It stands to reason that the one-photon detuning of the two parts of the light field must coincide ($\delta_L^{eg} = \delta_L^{eg}$). Under these conditions, deriving the relationship $G_{ge} = G_{g'e} = G_{efrom}$ condition 8 is conceivable. During synthesis, the G-coefficient of a generic

dark state is only affected by the excited states involved (not the ground states). When multiple dark states appear simultaneously, one can characterize each dark state's contribution to the overall signal by calculating G_e . The Zeeman and hyperfine structures of the ^{87}Rb atoms are accounted for by our model. The communication conspires, or the assortment of nuclear sublevels

associated with the arrangement of the dim state, is characterized in the segments that follow. To show how the Ge coefficients characterize the CPT reverberation strength, the results of applying the model to a confined decreased framework are given.

3.3 Simplified atomic system: analytical solution

I have used the method shown at the beginning of this section on Figure 3(a) to

demonstrate how the Ge coefficients can handle the CPT reverberation under the assumption that the six levels related to the collaboration are segregated. Comparative considerations should also be given to the CPT reverberation and figure 3(b). Figure 4 shows the schematic of the divided 6-level framework. The names of the Zeeman sublevels are short.

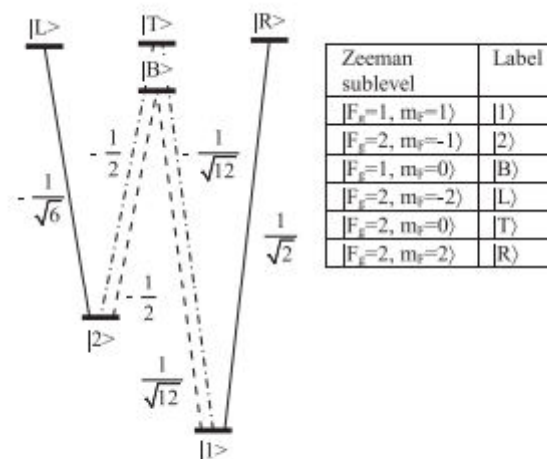


Figure 3: six-level excitation framework the dipole grid component for the advances, which are addressed as products of the Rabi frequencies V_{eg} , is the near the-progress coefficients, which are products of the coefficient.

$$V^0 = \sqrt{\frac{3\gamma_{SPC}^3 \hbar}{2\omega^3}}$$

In this part, I will give a synopsis of a method for deciding the CPT reverberation in view of the perception that conditions 3, 4, and 5 might be utilized to figure the light power consumed by the molecules, which is relative to the noticed sign. Based on a simplified 6-level system, I have analytically demonstrated that the destructive quantum interference effect of the ^{87}Rb excited state hyperfine structure plays a significant role in the CPT excitation process. It is found that the quality of this obstruction might be precisely portrayed by the proportion G_1/G_2 , which is delivered by the association between the optical lucidness rot rate γ' and the laser detuning, δL . Comparable (excitation) forces

in both dull states are communicated by a proportion that is close to solidarity, which brings about critical impedance and the retraction of the CPT reverberation.

4. EXPERIMENTAL SETUP

A drawing of the trial layout is shown in Figure 5. The lope is a few cm^3 glass cell that holds the ^{87}Rb isotope and N_2 as a support gas. Specifically, two identical cells with separate pad gas pressures of 0.5 and 1.5 kPa are utilized. The phone is maintained at $(68 \pm 1)^\circ \text{C}$ over this period, which corresponds to an optical progress Doppler expanding of $\Gamma D = 2\pi \cdot 540 \text{ MHz}$. Because both light fields are co-proliferating, the 6.8 GHz distinction recurrence causes the Doppler widening of



the CPT reverberation. Remember that in light of the fact that the molecules are held inside a volume that is essentially more modest than the 4.4 cm frequency that compares to the recurrence of 6.8 GHz, the miniature wave Doppler impact is fundamentally decreased by the Dicke limiting on account of a cushion gas cell. At a temperature of 68°C the ^{87}Rb cell ends up being optically thick. Thus, when a solitary mode laser (VCSEL or ECDL) is in reverberation, the cell conveyance, otherwise called the proportion of the laser power after the phone to the laser force before the phone (I/I_0) is dependably ≤ 0.3 which demonstrates that the optical thickness is under 1.

The laser radiation imparted through the telephone is assembled onto a photodetector (PD) whose sign is improved in a continuous speaker sometime later. Finally, the assortment (increase) of the optical

transmission is recorded by a modernized oscilloscope directly connected with the continuous enhancer. Moreover, the CPT resonance can be checked by including a lock-in speaker

The cell was set inside a CO-NETIC composite alluring shield to safeguard it from the effects of wrong alluring fields and alluring tendencies. To raise the debauchery of the Zeeman sublevels inside the protecting, a solenoid gave the longitudinal alluring field, $B_z = (3.0 \pm 0.2) \mu\text{T}$. Using the gJ dependence of the fringe CPT resonance, or the dull states made by the clarity of $|F = 1, mF = 0$ and $|F = 2, mF = \pm 2$, the alluring field has been continually checked during the tests. Contingent upon the useful block VCSEL or PL-Laser, the tests are done with either a current tweaked VCSEL or a PL-Laser.

101602

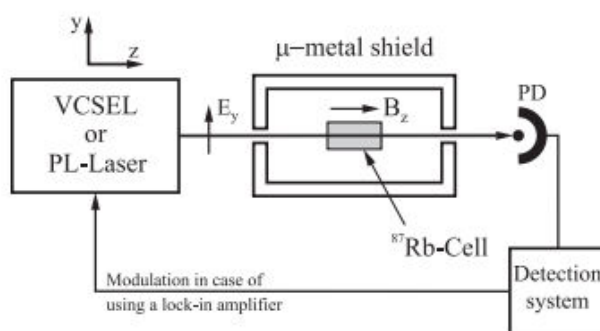


Figure 4: A block-style outline of the exploratory arrangement. All through the preliminaries, a balanced VCSEL and two PL-ECDLs filled in as substitute laser light sources. An ongoing enhancer, a computerized oscilloscope read by a PC, and a lock-in speaker (discretionary) make up the location framework block. The straightly delighted laser radiation's electrical field vector, E_y , is shown. An alluring field $B_z = 3 \mu\text{T}$ is applied in the tests toward laser transmission. a 2 mm ($1/e^2$).

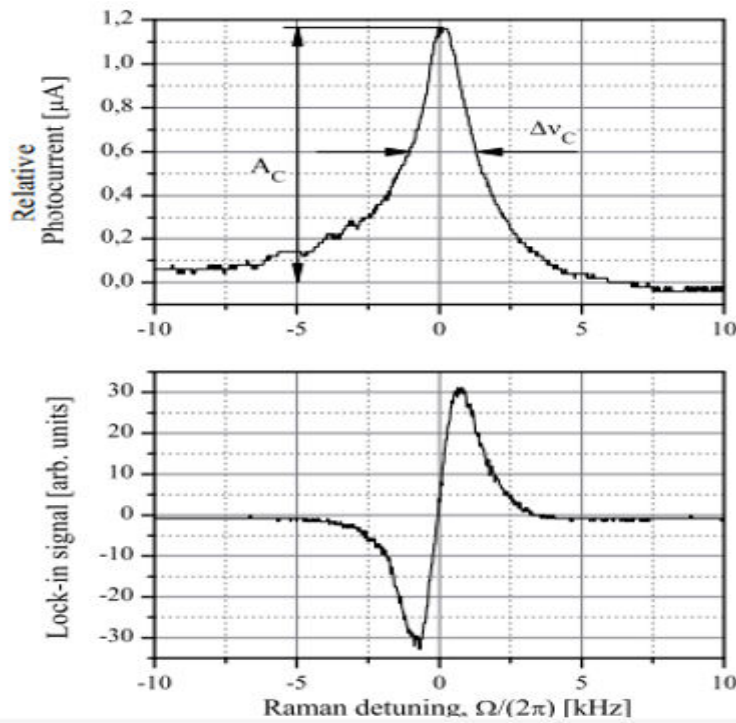
ECDLs. A 2 mm ($1/e^2$).distinction exists between the two laser frameworks. a Gaussian pillar profile and a bar midriff. It is vital for remember that the otherworldly linewidth, which is $\Gamma_V > 100 \cdot \Gamma_P L$, is the essential contrast between the two laser frameworks. Coming up next is a short depiction of the qualities of the two laser frameworks.

Modifiable VCSEL A singular mode VCSEL transmitting at 795 nm has its imbue ment current directly changed with 10 dBm of RF power at 3.417 GHz, or a major piece of the ground state hyperfine division in ^{87}Rb . The noticed linewidth VCSEL, $\Gamma_V \approx 2\pi \cdot 100 \text{ MHz}$

shows an expansive range. By moving the repeat and adequacy of the continuous change, the change execution has been reviewed using the one photon ^{87}Rb maintenance territory. The recurrence tweak record was assessed to be around 1.8, and we couldn't recognize any impact from plentifulness balance. The first-request side-groups utilized for dull state excitation are equitably dispersed, representing generally 68% of the complete laser yield under these circumstances. The carrier repeat and higher-demand sidebands get a large portion of the extra 32% of the general power. Considering the Doppler widening of the hyperfine

advances, these off-deafening regions of the VCSEL reach can achieve one-photon excitation processes. Besides, the photodetector's dc and shot upheaval levels are rising a direct result of the non-consumed off-full light. PL (stage locked) lasers the basic pieces of the PL-laser structure are two Widened Pit Diode Lasers (ECDLs), implied as the master and slave lasers. Both of these

ECDLs work at Γ ECDLs ≈ 0.5 MHz. furthermore, have a confined range. An extra cleared the 87Rb D1 line $5\ 2S_{1/2}\ F_g = 2 \rightarrow 5\ 2P_{1/2}\ F_e = 1$ progress, course of action settles the expert laser's 87Rb D1 line $5\ 2S_{1/2}\ F_g = 2 \rightarrow 5\ 2P_{1/2}\ F_e = 1$ change. The laser adjustment's fast servo circle meaningfully affects the line width.



101603

Figure 5: A representation of a run of the mill CPT resounding made utilizing PL-ECDLs and reverberation with the party of changes prompting $F_e = 1$ (laser force practically identical to $3.8\ \text{MW cm}^{-2}$). The lock-in signal (base) and the oscilloscope signal (top) are depicted. The CPT resounding has an adequacy of $\Delta C = 1\ \mu\text{A}$ and $\Delta v_C = 3\ \text{kHz}$, freely.

The standardized optical transmission varies by 4% due to the CPT. Realize that we record commonly 3% of normalized optical transmission difference under the vague conditions using a directed VCSEL. The presence of off-reverberation frequencies, which increment the power of the foundation light, causes the error. Of the master is on various occasions more unassuming. A heterodyne beat signal is used to organize lock the slave laser to the master laser. To recognize the 6.8 GHz beat expected for the tests, a fast photodiode superimposes the light points of support from the master and slave lasers. The heterodyne beat signal is intensified and afterward brought down to 50 MHz by a twofold adjusted ring blender, where it is contrasted with a reference

recurrence signal from a Moderate Recurrence (IF) oscillator. A stage/recurrence indicator produces a result signal that is relative to the stage distinction that exists between the down-changed over beat note and the IF-Oscillator. To stop the input, the stage finder's result signal is circled back to the slave laser. A mixed basic modernized stage locator is used in the arrangement. This method meanwhile achieves a wide catch reach and no man's sans land locking. The PL-arrangement's overall stage jitter, estimated in the recurrence scope of 1 Hz to 1 MHz, has the root mean square (rms) stage commotion level (relative stage jitter) of the PL-arrangement is $\Phi_{\text{rms}} \leq 50\ \text{m}_{\text{rad}}$ (estimated in the band of 1 Hz-1 MHz). To associate over the splitting of the 87Rb hyperfine ground states



because of PL-ECDLs, the repeat portions of the dichromatic electromagnetic field are secluded by 6.835 GHz. The immediate polarization state and powers are chosen to be undefined for the two repeat parts. To wrap things up, a polarization-safeguarding single mode fiber is utilized to guarantee that the two recurrence parts' collinear wave vectors are immaculate. A confuse in the wave vector forestalls a leftover extending of the CPT-resonances thus.

The photocurrent variance (top plot) and lock-in signal (base plot) for a standard PL-ECDL-made CPT reverberation are shown in Figure 5. The background photocurrent variance is the CPT reverberation sufficiency, or AC, in this study, and the full width at half maximum extreme (FWHM) of the reverberation is the CPT reverberation linewidth, or VC. I have used this interpretation of AC as our goal is the quantitative assessment of quantum obstruction between faint states. This system makes it conceivable to see the force of the CPT impact, which is affected by quantum impedance, and the light level in the tests, which shifts while involving PL-ECDLs or VCSELs considering the obligation of the changed VCSEL range at off-resounding frequencies. The analysis's use of the (foundation) light power, which primarily affects the Sign/Clamor Proportion, is important for applications and warrants further investigation. As previously described, the standardized optical transmission caused by the CPT impact is approximately 4% for PL-ECDLs and 3% for regulated VCSEL in the trial settings depicted in figure 5.

5. CONCLUSION

This study of the proposed CPT resonance focuses on the sign between ground state Zeeman sublevels such $mF = \pm 1$, which is a prospective opportunity for compact, believable atomic clocks. The indisputable features of this association plan stem from the quantum impedance between the dull states attained by the two stimulated hyperfine levels. Stunted development and laser linewidth of the atomic structure are taken into account while promoting a model. This study looks on the sign's energized state

hyperfine arrangement during laser detuning. The impact of each individual weak state on the CPT reverberation can be quantified by separating the model estimates from the exploratory disclosures. The ability to compute the impacts of the laser linewidth on the CPT resonance is finally eliminated, thanks to the strong quantitative knowledge of conjecture and evaluations.

REFERENCES

1. A. Lezama, S. Barreiro, A. M. Akulshin, *Phys. Rev. A* 59 (1999) 4732.
2. A. Nagel, K. Graf, A. Naumov, E. Mariotti, V. Biancalana, D. Meschede, R. Wynands, *Europhys. Lett.* 44, (1998) 31.
3. A. V. Taichenachev, V. I. Yudin, V. L. Velichansky, S. A. Zibrov, *Pis'maZhETF* 82, (2005) 449.
4. C. Affolderbach, S. Knappe, R. Wynands, A.V. Taichenachev, V. I. Yudin, *Phys. Rev. A* 65 (2002) 043810.
5. D. V. Kosachev, B. G. Matisov, Yu. V. Rozhdestvensky, *J. Phys. B* 25 (1992) 2473.
6. E. A. Korsunsky, N. Leinfellner, A. Huss, S. Balushev and L. Windholz, *Phys. Rev. A* 59 (1999) 2302
7. J. Kitching, L. Hollberg, A. V. Taichenachev, V. L. Velichansky, V. I. Yudin, *Laser Phys. Lett.* 1, 10, (2004) 257. G.A. Kazakov, I.E. Mazets, Yu.V. Rozhdestvensky, et.al., *Eur. Phys. J.D* 35, (2005) 445. A.B. Post, Y.- Y. Jau, N.N. Kuzma et.al., *Phys. Rev. A* 72, (2005) 033417. T.Zanon, S.Guerandel, E. de Clerq, et.al., *Phys. Rev. Lett.* 94, (2005) 193002. G. Kazakov, B. Matisov, I. Mazets, G. Mileti, J. Delporte, *Phys. Rev. A* 72, (2005) 063408.
8. J. Vanier, *Appl. Phys. B*, 81 421442 (2005).
9. K.Takagi , R.F. Curl , R.T.M. Su, *Appl. Phys.*, 7,(1975) 298. G.Alzetta, A.Gozzini, M.Moi, G. Orriolis, *NuovoCimento B* 36, (1976) 5. E. Arimondo, G. Orriols, *NuovoCimentoLett.*, 17, (1976) 333.



10. L. V. Hau, S.E. Harris, Z. Dutton, C.H. Behroozi, *Nature* 397, (1999) 594. G. P. Djotyan, *Opt. Exp.* 4, (1999) 113.
11. M. D. Lukin, S. F. Yelin, M. Fleischhauer, M. O. Scully, *Phys. Rev. A* 60 (1999) 3225
12. M. Rosenbluh, V. Shah, S. Knappe, J. Kitching, *Opt. Expr.* 14, 15, (2006) 6588.
13. R. Wynands, A. Nagel, S. Brandt, D. Meschede, A. Weis, *Phys. Rev. A* 58 (1998) 196.
14. S. E. Harris, *Phys. Today* 50, (1997) 7.
15. S. Knappe, M. Stähler, C. Affolderbach, A.V. Taichenachev, V.I. Yudin and R. Wynands, *Appl. Phys. B* 76 1 (2003) 57-63.

